AD-A195 249 STRUCTURING PROCESSES IN EXPANDING LASER-PRODUCED PLASMAS(U) NAVAL RESEARCH LAB WASHINGTON DC B H RIPIN ET AL. 30 MAR 88 NRL-MR-6154 1/1

UNCLASSIFIED F/G 9/3 NL

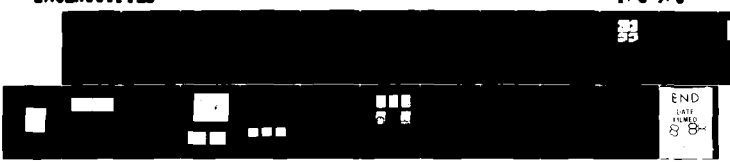

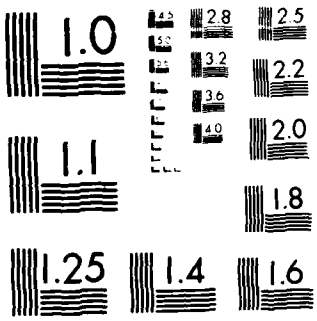

Naval Research Laboratory

Washington, DC 20375-5000

NRL Memorandum Report 6154

Structuring Processes in Expanding Laser-Produced Plasmas

B. H. RIPIN, J. GRUN, T. N. LEE, C. K. MANKA,
E. A. MCLEAN, A. N. MOSTOVYCH, C. PAWLEY,
T. A. PEYSER AND J. A. STAMPER

Plasma Physics Division

March 30, 1988

AD-A195 249

SECURITY CLASSIFICATION OF THIS PAGE

REPORT DOCUMENTATION PAGE

Form Approved
OMB No. 0704-0188

1a REPORT SECURITY CLASSIFICATION UNCLASSIFIED	1b RESTRICTIVE MARKINGS
2a SECURITY CLASSIFICATION AUTHORITY	3 DISTRIBUTION/AVAILABILITY OF REPORT Approved for public release; distribution unlimited.
2b DECLASSIFICATION/DOWNGRADING SCHEDULE	
4 PERFORMING ORGANIZATION REPORT NUMBER(S) NRL Memorandum Report 6154	5 MONITORING ORGANIZATION REPORT NUMBER(S)
6a NAME OF PERFORMING ORGANIZATION Naval Research Laboratory 6b OFFICE SYMBOL (If applicable) Code 4730	7a NAME OF MONITORING ORGANIZATION
6c ADDRESS (City, State, and ZIP Code) Washington, DC 20375-5000	7b ADDRESS (City, State, and ZIP Code)
8a NAME OF FUNDING SPONSORING ORGANIZATION Defense Nuclear Agency 8b OFFICE SYMBOL (If applicable) RAAE	9 PROCUREMENT INSTRUMENT IDENTIFICATION NUMBER
8c ADDRESS (City, State, and ZIP Code) Washington, DC 20305-1000	10 SOURCE OF FUNDING NUMBERS PROGRAM ELEMENT NO: 47-1606-0-8 PROJECT NO: RB RC TASK NO: 00168 WORK UNIT ACCESSION NO

11 TITLE (Include Security Classification)

Structuring Processes in Expanding Laser-Produced Plasmas

12 PERSONAL AUTHOR(S) Ripin, B.H., Grun, J., Lee, T.N., Manka, C.K., McLean, E.A., Mostovych, A.N., Pawley, C., Peyser, T.A., and Stamper, J.A.

13a TYPE OF REPORT	13b TIME COVERED	14 DATE OF REPORT (Year, Month, Day)	15 PAGE COUNT
Interim	FROM _____ TO _____	1988 March 30	24

16 SUPPLEMENTARY NOTATION

17 COSATI CODES			18 SUBJECT TERMS (Continue on reverse if necessary and identify by block number)
FIELD	GROUP	SUB-GROUP	Plasma, Turbulence, Rayleigh-Taylor, Laser-Produced Plasma, Structure

19 ABSTRACT (Continue on reverse if necessary and identify by block number)

A plasma expanding into a magnetic field and/or another plasma can undergo several instabilities which will cause spatial nonuniformities and large scale structure to develop. Potential structure forming instabilities include: various forms of the Rayleigh-Taylor or interchange instability, Kevin-Helmholtz instabilities. In addition, experimental geometric factors can also affect expansion uniformity. The phenomena reported here should be of interest to a broad range of disciplines.

20 DISTRIBUTION/AVAILABILITY OF ABSTRACT	21 ABSTRACT SECURITY CLASSIFICATION
☒ UNCLASSIFIED/UNLIMITED ☐ SAME AS RPT ☐ DTIC USERS	UNCLASSIFIED
22a NAME OF RESPONSIBLE INDIVIDUAL Barrett H. Ripin	22b TELEPHONE (Include Area Code) 202-767-3379 22c OFFICE SYMBOL Code 4732

DD Form 1473, JUN 86 Previous editions are obsolete SECURITY CLASSIFICATION OF THIS PAGE

S/N 0102-LF-014-6603

CONTENTS

STRUCTURING PROCESSES IN EXPANDING LASER-PRODUCED PLASMAS

INTRODUCTION

A plasma expanding into a magnetic field and/or another plasma can undergo several processes which will cause spatial nonuniformities and large-scale structure to develop. Structure forming instabilities include various forms of the Rayleigh-Taylor instability or interchange instability, Kelvin-Helmholtz instability, universal instabilities, and streaming instabilities. In addition, geometric and plasma production factors can affect expansion uniformity.

In this article, we describe experiments in which plasma nonuniformities arise when laser-produced plasmas expand into other ambient plasmas and/or magnetic field regions. Several types of density structure appear, depending upon the operational regime.[1] Dramatic large-scale flutes grow when the laser-plasma expands into a vacuum magnetic field or a low-density magnetized plasma. The mechanism has been identified as a type of Rayleigh-Taylor or interchange instability occurring in a relatively unexplored regime where the ion Larmor radii are large.[2,3] Plasma jetting across magnetic fields has been studied. This is caused by polarization drifts arising when gross asymmetry is present.[4,5] When the laser-produced plasma expands into a high pressure background-plasma or gas, collisional blast-waves are formed. Several structure-forming mechanisms occur here also. Aneurisms,[1,6] which are protrusions from the otherwise smooth blast-fronts, often appear; several mechanisms are responsible for these unusual projections, among them effects associated with the incoming laser-beam deposition[6] and material jetting normal to the target.[7] Finally, it has recently been shown that ablatively accelerated foils undergo Rayleigh-Taylor (R-T) instability during laser irradiation.[8] These R-T unstable accelerated thin-foils continue to develop gross turbulence as they expand into a vacuum or background gas. The measured turbulence has been Fourier analyzed to yield power spectra at successive times in the expansion phase.[9]

Manuscript approved December 22, 1987.

In the remainder of this article, we will describe these structuring processes in more detail. These phenomena are, for the most part, not unique to laser-produced plasmas and should be applicable to a broad range of disciplines. Our results are related to problems in space physics, magnetic confinement/fusion, laser-guided particle beams, ICF reactor design, and basic plasma physics.

EXPERIMENTAL ARRANGEMENT

The experiment consists of an energetic laser-produced plasma expanding into a vacuum and/or a photoionized gas as depicted in Fig. 1. Details of the basic experimental arrangement and earlier results have been published elsewhere.[1] The energetic laser-produced plasma is formed by placing a small target, typically a 1 mm or less diameter and 2 μm thick aluminum disk, at the focus of one or two beams of the PHAROS III Nd-glass laser. Laser pulse durations of 3 to 5 ns, energies up to 400 J/beam, irradiances of 10^{12} to 10^{14} W/cm^2, and spot diameters between 0.25 and 1 mm are used in the present studies. Laser-produced ablation plasmas having initial temperatures of 500 to 1000 eV are formed; these expand radially away from the focal region and reach asymptotic speeds of 5 to 8 x 10^7 cm/s within a millimeter to two. If a background gas is introduced, it is partially photoionized by the X-ray and UV emissions of the laser-plasma interaction. A magnetic field up to 11 kG is often impressed on the entire system by means of a pulsed set of 25 cm diameter Helmholtz coils; the magnetic field is effectively steady-state during the relevant part of the experiment.

A large array of instruments are used to measure the plasma properties and dynamics. Diagnostics include ion time-of-flight detectors, magnetic-field induction probes, diamagnetic loops, multi-time dark-field optical shadowgraphy, interferometry, Langmuir and capacitance probes, x-ray detector arrays, fiber-optic/OMA spectroscopy systems, and more. Most of these diagnostics are described in detail in Ref. 1. There are two notable additions. A fast-gated (120 ps < Δt < 5 ns) Grant Applied Physics microchannel plate S-25 optical camera (dubbed a GOI, gated optical imager) is used to obtain high-resolution time-resolved images of low-density plasma interactions. This instrument is used to image the plasma structure in low density situations, such as those encountered in the next section. The other new diagnostic is a resonant laser probe, which is also useful in low density plasmas. The resonant probe beam comes from a dye laser, pumped with a 5-ns duration frequency-doubled Nd-laser, which is tuned to either the wing or center of a plasma ion-resonance line. Index of refraction enhancements of 1000 over the usual electron contribution are possible using this technique. One form of plasma jets, to be discussed later, was found using this technique.

LARGE LARMOR RADIUS INTERCHANGE INSTABILITY

Plasma expanding into a magnetic field can undergo Rayleigh-Taylor or interchange instability as the heavy fluid (plasma) is decelerated by the light fluid (magnetic

field).[10,11] This instability has been observed in experiments where MHD theory is valid, namely, where the ion Larmor radius is small with respect to density gradients and instability wavelengths.[12-14] When the ion Larmor radius becomes larger, i.e., comparable to density gradient scale-lengths, the instability is predicted to stablize,[15] although no experimental verification of this has yet been made. Recently, however, it has been predicted that when the ion Larmor radii are very large (i.e., the ions are effectively unmagnetized, but the electrons remain magnetized) the instability not only reappears, but exhibits a much faster growth and different character than the ordinary MHD Rayleigh-Taylor version.[2,16] The recent AMPTE Barium release space experiment, which also showed structuring, was in such a regime.[17]

We observe a robust interchange-like instability in the very large ion Larmor radius limit.[3] The instability exhibits a rapid linear phase with subsequent nonlinear freestreaming flutes and examples of density clumping, flute-tip bifurcation, and interesting late-time spiral-like structures.

Our experiment[3] is comprised of an energetic laser-produced plasma expanding radially outward into the uniform magnetic field, as depicted in Fig. 1. Vacuum B-fields from zero to one Tesla are used. Plasma bursts are created by focusing one or two beams of the PHAROS III Nd-laser onto small Al (2 μm thick, 1 mm diameter) disk targets. Unless noted otherwise, the nominal laser pulse has an irradiance of about 10^{13} W/cm^2, 30 J of energy, and 3 ns duration (FWHM). The principle diagnostic used to measure the plasma and instability development is the previously described GOI microchannel plate camera focused onto the target mid-plane antiparallel (usually) to the magnetic field lines. Shutter speeds of 1 or 2 ns are used. In addition to the gated camera, we also used: ion time-of-flight detectors to measure the plasma ion velocity distribution; several small (230 μm dia., two-turn) magnetic induction probes to obtain magnetic field dynamics; small Langmuir and capacitive probes to measure density gradients and fluctuations; open-shutter photography and witness plates to see persistent structure; and fiber-optic spectroscopy used to estimate density profiles during the plasma/magnetic field interaction.

The velocity distribution of the expanding plasma, measured with zero magnetic field, peaks at $V_o \approx 5.4 \times 10^7$ cm/s with a FWHM spread of $\pm$ 1.8 x 10^7 cm/s. The total plasma mass is about $m_o = 0.2$ μgm (half of which is directed into the front $\pm$ 45° expansion cone), the initial electron temperature is about 500 eV, and the aluminium ionization state is approximately 10. Thus, the ion Larmor radii are large, over 1.6 cm for 1.0 Tesla and over 16 cm for B=0.1 Tesla (assuming Z is ten or less). The electrons, on the other hand are effectively magnetized with Larmor radii below one millimeter. Most of the experiments were performed with ambient pressures below 0.1 mTorr so that the magnetic field dominates the plasma expansion. The plasma

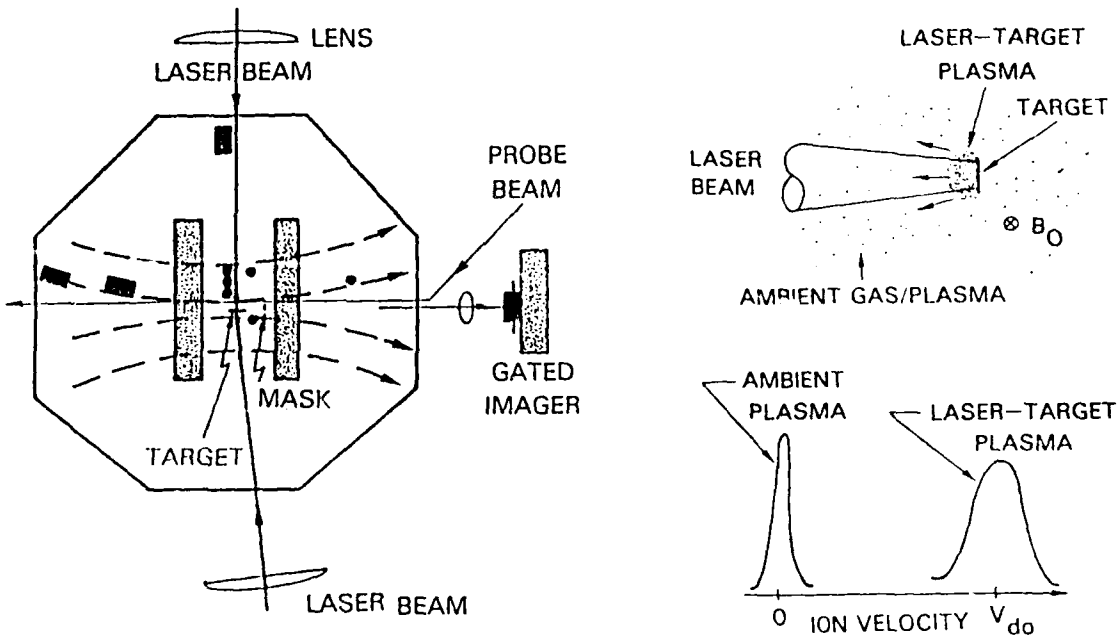

Figure 1. Arrangement for laser-plasma structure experiments.

expansion speed is very subAlfvenic, being more than one order-of-magnitude slower than the maximum possible Alfven velocity in the residual background air.

In an external magnetic field, the expanding plasma decelerates as it excludes magnetic field energy. Ideally, a symmetric plasma expansion would stop near the "magnetic confinement" radius, R_b, where the excluded field energy equals the original plasma energy. For the typical 30 J shot in our experiment, R_b is 3.3 cm for B=1 Tesla and 15 cm for B=0.1 Tesla. The plasma decelerates with $g \approx -5 \times 10^{14}$ cm/s^2 at R=3 cm for B=1 Tesla, as seen in Fig. 2b. The deceleration is less apparent in the 0.1 Tesla experiments, Fig. 2a, since we observe it for $R < R_b$. At intermediate magnetic field values the observed magnetic confinement distance follows the expected $B^{2/3}$ dependency within the data error bars ($\pm$20%).[18,19] The plasma continues to diffuse across the magnetic field beyond R_b, but at reduced speed, a consequence, perhaps, of our lack of a totally symmetric expansion.

The density scale-lengths of the plasma fronts in a magnetic field at about 3 cm from the target fall in the range $L_n = 10 \pm 3$ millimeters. These estimates were obtained from the emission profiles of the time-resolved optical images, the risetimes of the Langmuir and potential probe signals, and the risetime of spatially and temporally resolved Al^{+2} line (361.2 nm) emission.[20,21]

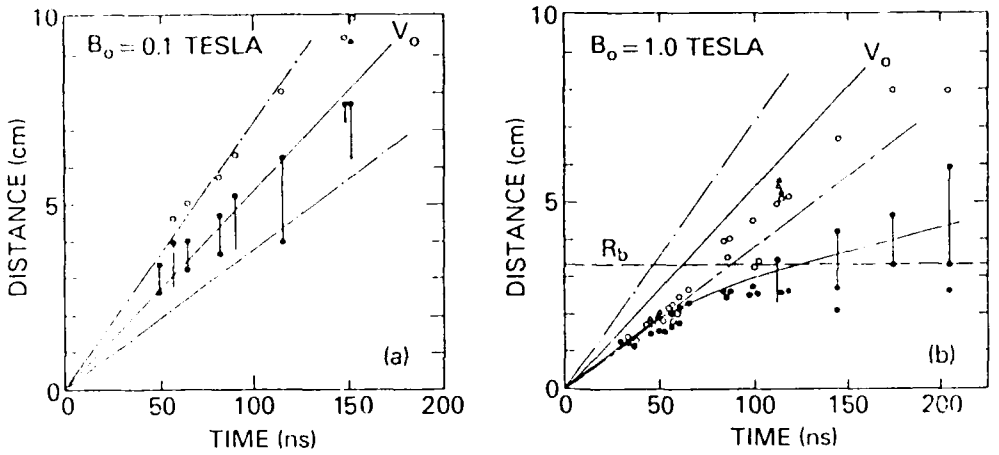

Figure 2. Development of the plasma expansion and instability. Locations of the instability spike tips (o) and main plasma boundaries (●) with time for the low (0.1 Tesla) field case (a) and the high (1.0 Tesla) field case (b). Shots denoted by a Δ are plasma boundaries with zero applied magnetic field (freestreaming plasma). E_i = 25-30 J, $V_o = 5.4 \times 10^7$ cm/s, and P<0.1 mT for all cases.

An array of magnetic field probes located at 1, 2, 3, 4, and 5 cm from the target show a very small (few percent at most) magnetic compression ahead of the plasma front followed by a greater than 30% diminished field within the plasma front. This field behavior is generally consistent with subAlfvenic plasma expansion with, perhaps, a higher than classical resistivity leading to a magnetic diffusion length, $L_b \approx c/\omega_{pi}$.

Before the plasma reaches R_b, structure develops in the plasma leading (outer) edge. Distinct plasma flutes project out from the main plasma body into the magnetic field, as shown in Fig. 3. The initial development of the instability can be seen in the low (0.1 Tesla) case shown in Fig. 2a. During the first 50 ns ($R < R_b/5$), the plasma expands with speeds near V_o and no sign of instability is discernible; suddenly, near R = 3 cm, radial plasma projections appear with amplitudes comparable to their wavelengths 5 ± 1 mm. It is clear from the distance versus time plot, that these plasma tips then continue to freestream outward into the magnetic field. Since $R << R_b$ the bulk plasma is also still expanding close to its intial speed. Curi usly, despite a much stronger deceleration in the 1 Tesla case ($g \propto B^2$), the instability also begins to develop at about the same distance and time as in the lower field case (see Fig. 4). This onset behavior is consistent with the instability criterion[16] $g/L_n > \Omega_i^2/4$, which is independent of the magnetic field; Ω_i is the ion cyclotron frequency. The instability wavelengths turn out to be also independent of the magnetic field strength. The flute amplitude grows rapidly after onset with a linear growth rate above 10^8 s^{-1},

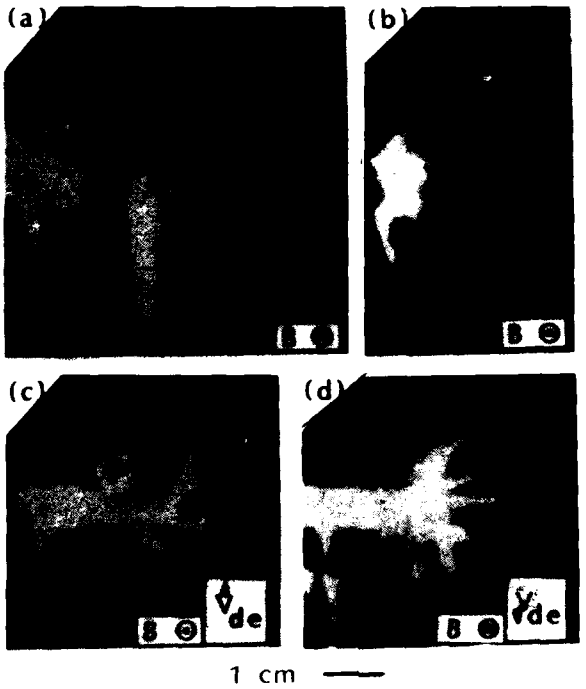

Figure 3. Examples of the instability development. (a) 0.1 Tesla case observed at time 115 ns. (b) Example of density clumps in the early-time phase development with B = 1.0 Tesla at time 59 ns. (c) Example of curved spike structure with with 1.0 Tesla field (field points out of paper) at 115 ns. (d) Same as (c) except field points into paper and t = 100 ns; note reversal of curvature sense. E_1 = 25-30 J and P< 0.1 mT for these shots.

as seen in Fig. 4. Unfortunately, the accuracy of the growth rate measurement (factor of two) is limited by the shot-to-shot reproducibility of the onset time. For comparison, the conventional (small ion Larmor radius) MHD Rayleigh-Taylor growth rate ($\gamma = (g/L_n)^{1/2}$ for $kL_n > 1$) for our parameters (B = 1 T) is only about 2 x 10^7 s^{-1}, whereas the large Larmor radius instability theory[2] predicts a six times faster growth rate for the observed wavelengths, consistent with our experimental result. At times, the plasma structure initially appears as density clumps in the leading edge of the expansion plasma. This clumping-like behavior, shown in Fig. 3b, is a predicted characteristic of this instability.[2,16] Subsequent to the rapid linear phase of the instability the flute tips freestream with speeds near V_o.

The wavelengths of the predominant flute modes (measured at the base of the flutes) are typically about 5 mm and are also insensitve to most parameter changes. As time goes, on the instability wavelength tends to remain constant even though the plasma continues to expand radially. Thus, the

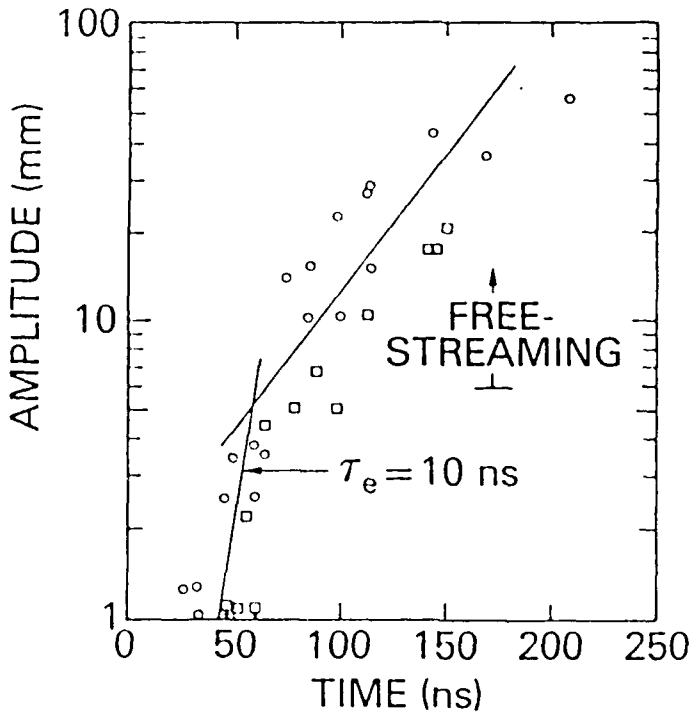

Figure 4. Onset and growth of instability flutes. Flute-tip-to-bubble amplitudes versus time for the 1.0 Tesla (o) and 0.1 Tesla (□) data of Fig. 2. Note that the onset time for both field values occurs near 50 ns and the linear growth e-fold time for the B=1 T data is about 10^{-8}s.

effective mode-number increases with radius. Some indication of how this can occur was obtained by placing witness plates (black Polaroid film) perpendicular to the magnetic field a few centimeters to one side of the target. These recorded time-integrated patterns of the plasma running down the field lines. Long spikes are seen in the exposures with curvature toward the midplane and additional projections formed towards the sides of the pattern with increasing distance from the source. The fact that the patterns on the witness plate are not washed out indicates that the plasma structure, once formed, does not undergo much azimuthal motion. Several examples of flute-tip bifurcation are also seen in the time-resolved GOI images,[18,19] such as shown in Fig. 5. The combination of these two effects tends to maintain constant wavelength and increase the instability mode number, $m = 2\pi R/\lambda$, with distance.

The dominant instability wavelength may be determined by the bulk plasma density scalelength, $L_n = 10 \pm 3$ mm, or possibly by the magnetic diffusion length into the plasma front, $L_b = 10$ mm. The collisionless skin (c/ω_{pe}) depth is only a fraction of a millimeter, but possible anomalous resistivity associated with this or another instability could push the diffusion length into the centimeter (c/ω_{pi}) range.

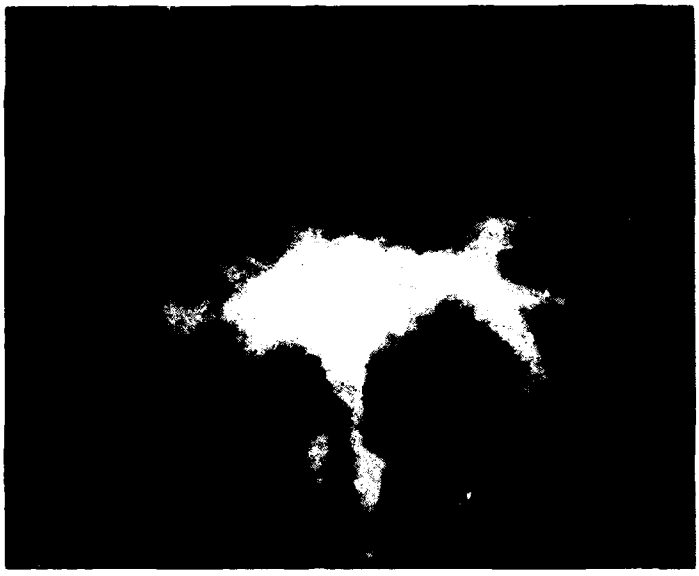

Figure 5. Example of LLR-instablity flutes undergoing bifurcation observed at t≈100 ns, B=1 T, with the GOI.

For some shots, the magnetic field was rotated 90° so that the instability development could be viewed perpendicular to the field lines. The plasma projections, which have the appearance of slim spikes in the end-on view, actually run smoothly along the field lines, confirming the flute-like geometry of the instability.

The freestreaming flutes exhibit some interesting features at later times. One common characteristic in the high field experiments is the curvature and spur-like appearance of the instability fingers seen in Figs. 3 and 5. The flute curvature is in the electron cyclotron or electron E x B drift sense and reverses with magnetic field direction. It is not yet known whether the curvature arises from the spike tips moving upward or the bubble downward. Two possibilities are that curved flutes are caused either by E x B or ∇ B x B induced electron velocity shear.[18,19]

A number of other parameter variations were performed during the course of this investigation. The background pressure was increased up to 2 Torr of H_2 to test the effects of increasing collisionality and decreasing Alfven speed on the instability. For the 0.1 Tesla case, viewed at 150 ns, freestreaming structure persisted up to 100 mTorr H_2 pressure at which point signatures of collisional effects were seen.[1]

In another series of shots, a 7.6 cm diameter, 3 mm thick copper disk was placed 4 to 5 cm to one side of the target, perpendicular to the field lines, to short out the dynamic motion of the magnetic field lines. The gross features of the instability persisted independent of whether the copper plate was grounded, ungrounded, insulated or bare.

Finally, several shots were taken with much larger incident laser energy (400 J) but comparable irradiance at a variety of magnetic fields and pressures. The major effect of higher laser energy is to proportionally increase the plasma mass and, hence, increase the magnetic confinement radius by $R_b \propto E_l^{1/3}$.

Another interesting observation in these experiments was the presence of a strong high-frequency (>250 MHz) signal seen in the plasma front by electrical and magnetic probes whenever the Rayleigh-Taylor instability occurred. This noise is in the ion-plasma or lower-hybrid frequency range. The relationship of this noise to the magnetic instability is not yet clear, but may be due to the growth of very short wavelength Rayleigh-Taylor modes, which cannot be seen in the framing pictures, or to the generation of microinstabilities in the plasma shell.[14,21,22]

CROSS-FIELD JETTING

If a blob of plasma is projected across a magnetic field with velocity V, then charge can accumulate on its boundaries due to polarization forces within the plasma. The polarization arises from the V x B forces on the electron and ion distributions as shown in Fig. 6. The charge separation in turn sets up a polarization electric field E which then allows the bulk of the plasma mass to E x B drift across the magnetic field near the original speed V. There are, of course, necessary conditions for this to occur; for one, the charges at the boundary need to be replenished, as they are peeled off and left behind the main plasma by the fringe polarization electric fields. Also, since energy is dissipated by the internal currents, the plasma jet will eventually stop. A good discussion of these criteria is given in Borovsky.[23] The plasma jet tends to form a sharp wedge when viewed end-on to the magnetic field, due to electric field gradients and curvature. A wedge-shaped plasma jet was previously noted by Jellison and Parson.[5] On the other hand, the plasma should fan out in the plane containing the magnetic field lines.

Fig. 6 also shows an excellent example of a Barium plasma jet viewed in absorption with our resonant probe diagnostic. This shadowgram was taken with the dye laser tuned to near the center of the 450 mm BaII ion line at a time of about 750 ns.[4] The jet is moving across the 10 kG field at its initial speed of 10^6 cm/s. The expected characteristic wedge-shape phenomena view and along B is very prominant. However, the view across the magnetic field is surprising indeed! The plasma is fanned out as expected, but remarkable fishbone-like structure is observed along the field lines.[4] A more detailed account can be found in Ref. 4.

Plasma jets have been formed several other ways in our experiment by creating asymmetric expansions. Fig. 7 shows two examples of such jets. The left side of Fig. 7 shows two jets resulting from plasma expansions of the type described in the last section. To induce jets, rather than the large Larmor radius instability, we put a cylindrical shield with a radius of about 1 cm about the target with slots cut in it to only allow two thin plasma sheets to pass through. In the example on the right side of Fig. 7, high-

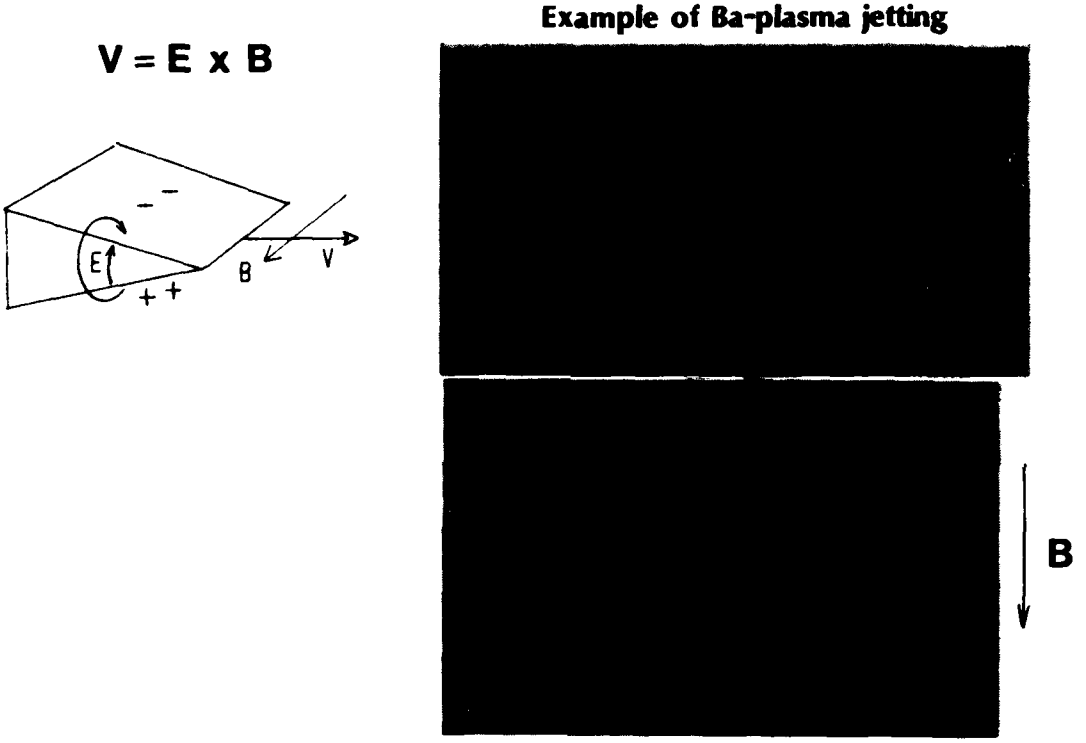

Figure 6. Cross-field jetting model and a laboratory example. The change separation and E x B drift models are illustrated to the left. On the right, an example of Ba-plasma jetting in a 1-T field is seen. The characteristic wedge shape (top) and "fish bone" instability (bottom) are seen.

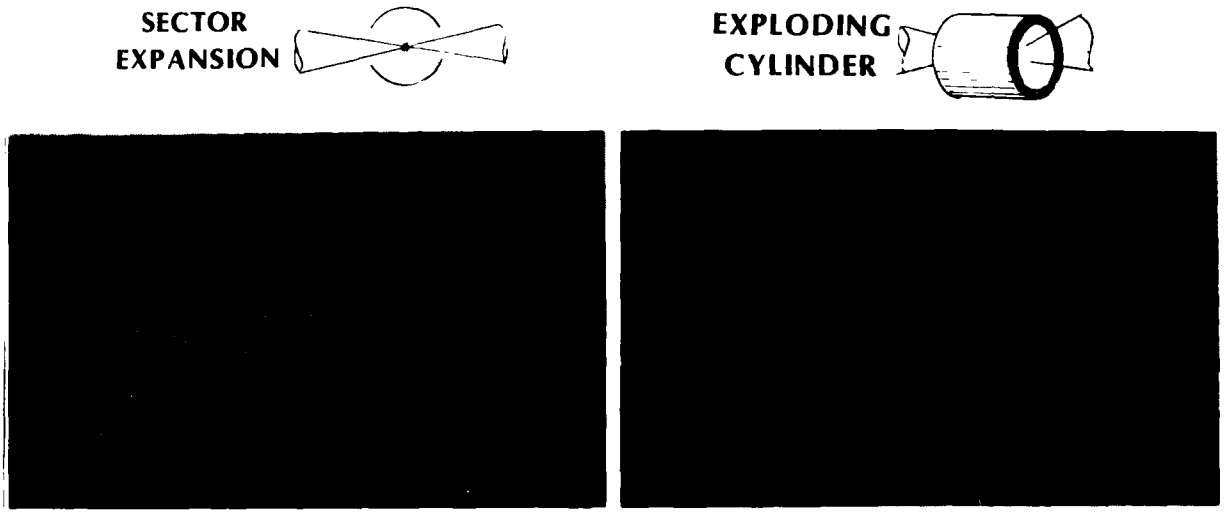

Figure 7. Two examples of laboratory jetting induced by geometric asymmetry. (left) A 30 J/beam two-beam expansion with a cylinderical shield [t=90 ns]. (right) A 100 J/beam two-beam shot into a cylinderical glass target [t=1 μs].

density, low-temperature jets are formed in an entirely different way.[24] Two oppositely-directed laser beams were focused into the ends of a glass cylindrical target (1 mm diameter, 2 mm long and with 50 μm wall thickness) causing dense plasma plumes to squirt out the cylinder ends across the applied magnetic field (10 kG in this case). Note that the observation time here is 1 μs after the laser pulse. Highly directed jets are seen crossing the field in both directions followed by masses of slower ($V = 3 \times 10^6$ cm/s) plasma.[24] Curiously, the slower plasma blobs seem to be fluting in a similar manner to the large Larmor radius instability as they move across the field.

A more detailed discussion of the important subject of cross-field jetting and these experiments will appear elsewhere. Jetting phenomena are important wherever plasma masses are projected across magnetic field regions such as in several astrophysical situations.[25]

STRUCTURE ASSOCIATED WITH COLLISIONAL PLASMAS

When a background gas is introduced around the laser-produced plasma, interactions between the expanding plasma and the stationary background plasma and gas are possible. At low gas pressure (below 100 mTorr), these interactions are collisionless beam/beam type instabilities.[1] Above about 1-Torr pressure, the interactions are collisionally dominated. A transition occurs between these two regimes. Fig. 8 shows a typical high-pressure dark-field shadowgram. Thin steep blast-waves are the dominant feature.[1] Several additional phenomena are also evident, such as aneurisms, large-scale turbulence regions behind the target, and a

turbulent region inside the blast front. We have recently established the mechanism causing on-axis aneurisms to be laser channel heating,[6] and this will be discussed below. The nature of the gross turbulence appearing behind the target will be discussed in the following section.

Aneurisms

Aneurism-like protrusions have been seen in several different laser-plasma experiments.[1,26] They frequently appear along the incident beam axis and near the target surface normal, although they are also seen at other angles as well.[1] A number of mechanisms have been suggested to explain these aneurisms including laser beam channel heating of the ambient gas,[27] jetting material from the target,[28] Rayleigh-Taylor instability of the blast front,[1] and magnetic field/thermal ablation process of the blast-wave interior.[29] We have recently discovered that several of these processes do occur, causing similar appearing, but different type, aneurisms.

Aneurisms aligned with the incident laser beam, such as shown in Figs. 8 and 9, are usually caused by laser heating of a channel in the ambient gas.[6] This phenomena would be of importance in proposed ICF reactors[30] in which a buffer gas is used to protect the first-wall against prompt x-ray and debris heating. Laser or particle beams would also create heated channels in the gas which could cause material in the aneurisms to be aimed at the last focusing optic, an undesirable effect.

The channel and resulting aneurism is formed as follows.[6] The UV and X rays from the laser-plasma interaction at the solid target photoionize the nearby gas. Fractional ionizations of a few percent are typical 1 cm from the target for 100 J incident energies and 5 Torr nitrogen gas pressures; the radial dependence of the ionization goes as approximately $1/r^2$. A very small fraction (0.4%) of the incident beam is absorbed in this low density plasma via inverse bremsstrahlung. The plasma in the laser channel quickly heats up to about 100 eV out to beyond 1 cm; this hot plasma expands radially in a cylindrical blast-wave causing a reduced density channel along the laser-beam axis. Later, the material swept up into the spherical blast-wave from the expanding target material is slowed less in the low density channel than off-axis and causes the aneurism protrusion.

We have established this mechanism experimentally by tilting the target 30% to separate the laser axis from the target normal and noting that aneurisms usually form along the laser-beam axis for higher energy (E_L > 10 J) shots at multi-Torr pressures. Additionally, we have found that target thickness and diameter, different laser focal-spot diameters, hot-spots, or ultra-smooth ISI focal spots[31] do not affect these on-axis aneurisms. We have observed the cylindrical shock formed by the superheated channel soon after the incident laser pulse is over; from its motion we infer that about 1% of the incident laser beam energy is

Figure 8. Blast-wave associated structure seen in dual-time shock-front shadowgrams (55 and 160 ns) of a 5 T N_2 ambient pressure shot. (36 J on a stalk mounted Al target).

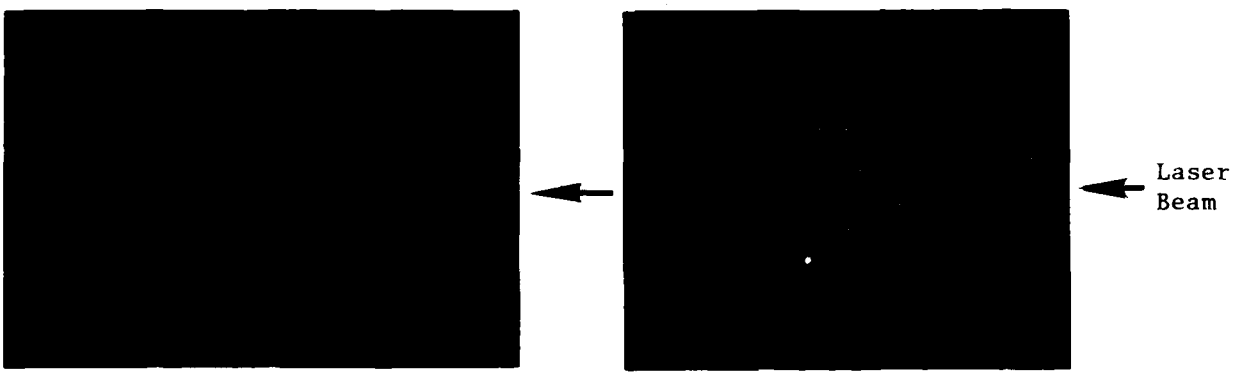

Figure 9. Example of pronounced on-axis beam-heated aneurism (5 T N_2, 109 J, t=71, 146 ns) (left) and cylinderical blast-wave (5 T N_2, 245 J) (right) formed by expansion of the beam-heated plasma at early time (14 ns).

invested in the channel formation, in agreement with theory and 2D computer simulations.[6] Quantitative agreement has been obtained between most aspects of the experiment and the corresponding theory/computer simulation; the reader is directed to Ref. 6 for more details.

Fig. 10 shows other examples of aneurisms where mechanisms other than beam channel heating must be operating. Aneurisms formed at lower incident energy near the normal to the target surface, as in Fig. 10a, appear to be caused primarly by target material jetting. Slow masses of target material, perhaps ejected after the incident laser pulse is over or from the region surrounding the focal region, catch up to the decelerating blast-front and punch out an aneurism. Evidence for jetting comes from framing camera pictures of the blast-wave system, taken with interference filters at specific Al II and Al III emission lines. These pictures show directed jets of Al target material inside the blast-front pushing out an off-axis aneurism.

Occasionally, turbulent appearing aneurisms are observed, such as shown in Fig. 10b. A cause of these aneurisms could be Rayleigh-Taylor instability of the blast-front.[1] Ordinarily, blast-waves are thought to be stable against hydrodynamic instability. But, if the blast-wave density profile is modified by radiation cooling or thermal conduction effects, adverse density gradients (oppositely directed density gradient and deceleration vectors could result. Classic Rayleigh-Taylor growth rates of about 10 ns [$(kg)^{1/2}$] are sufficient to explain the observed structure.[1]

Aneurisms also appear at angles other than the target normal and incident beam directions, such as shown in Fig. 10c. These aneurisms may be caused by ejection phenomena

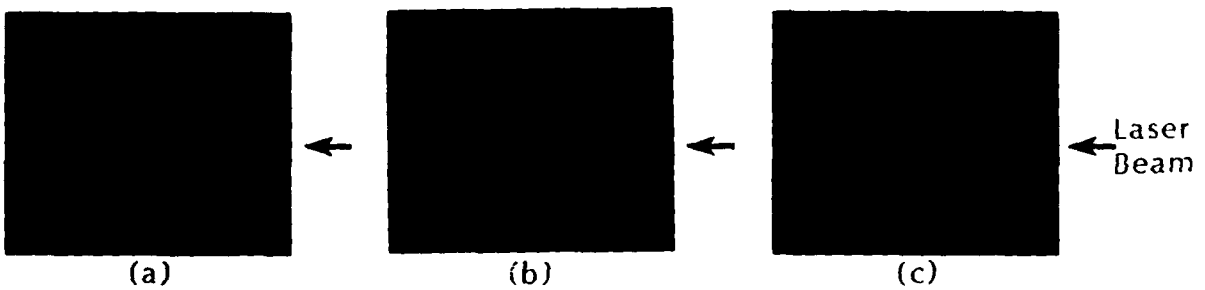

Figure 10. Examples of aneurisms not formed by the on-axis beam-heating mechanism. (a) Example of an aneurism probably directed about the target normal (30° from the laser axis) which is probably formed by plasma jetting. (35 J, 5 T, N_2 t=59 ns) (b) Turbulent appearing aneurism, perhaps caused by blast-wave Rayleigh-Taylor instability. [20 J, B=600 G, 7=1.5 Torr (90% N_2 + 10% H_2, t=52, 169 ns] (c) Odd-angle aneurism, perhaps caused by mechanism postulated by Giuliani, ref. 29. [38 J, B=0, 5 Torr, (90% N_2 + 10% H_2), t=52, 16 ns].

or, alternatively, by the thermal conduction model of Giuliani.[29] This model depends upon there being a hot plasma inside the blast-front. Imbedded in the blast-front are azimuthal magnetic fields, of order 1 kG, which originate either in the initial laser-plasma interaction[32] or are created in the expanding shock $\nabla n \times \nabla T$ gradients.[33] The magnetic fields inhibit the heat conduction to the blast-front except near the axial null of the azimuthal fields. The enchanced ablation in this region will both thin and accelerate this portion of the blast-wave to form an aneurism. Quantitatively, this process is consistent with all known experimental parameters,[29] but no direct verification has yet been made of its validity.

Dense Target Disassembly

The turbulence formed by the target material expanding away from the laser beam direction is especially striking as seen in Fig. 8. This material is dense target foil material which has been accelerated in reaction to the ablation plasma created on the laser side of the target.[34-36] It has been demonstrated that ablatively accelerated foils, such as used in these experiments, undergo Rayleigh-Taylor (RT) instability by the target acceleration g (of order 10^{15} cm/s^2) during the laser pulse duration.[8] Growth rates of about 60% of the classical $[(kg)^{1/2}]$ rate have been measured in detail by Grun et al.[37] An interesting question is whether the turbulence which is seen long after the laser pulse has ended is dominated by the RT created during the laser pulse? To answer this question, we create a dominant RT mode by using a grooved target and compare the resulting structure to flat targets as successively later times after the laser pulse.

Fig. 11 shows a compilation of such a sequence. The top row shows shadowgrams at various times when a 100 μm grooved target was accelerated. The bottom row is the same as the top row except that the target is a smooth flat foil of the same thickness. The 100 μm perturbed targets undergo RT growth during the laser pulse. Although, some residual remnants of the original 100 μm perturbation may be present after 80 ns, it is clear that the dominant structure is of much higher mode number and is largely independent of whether the target had an initial perturbation or not. Turbulent regions of the shadowgrams have been digitized and Fourier analyzed showing that they have similar spectral properties.[9] It has been suggested by Stamper that the dense target may undergo a Benard-type hydrodynamic instability causing the short-wavelength turbulence. The Benard instability would occur between a hot surface (laser side of the target is several hundred eV in temperature) and a cold surface (rear of target is known to be only a few eV) when an adverse acceleration direction is present. However, definitive demonstration of the cause of this turbulence, its long term time dependence, and the possible interaction with the background plasma/gas still needs to be determined.

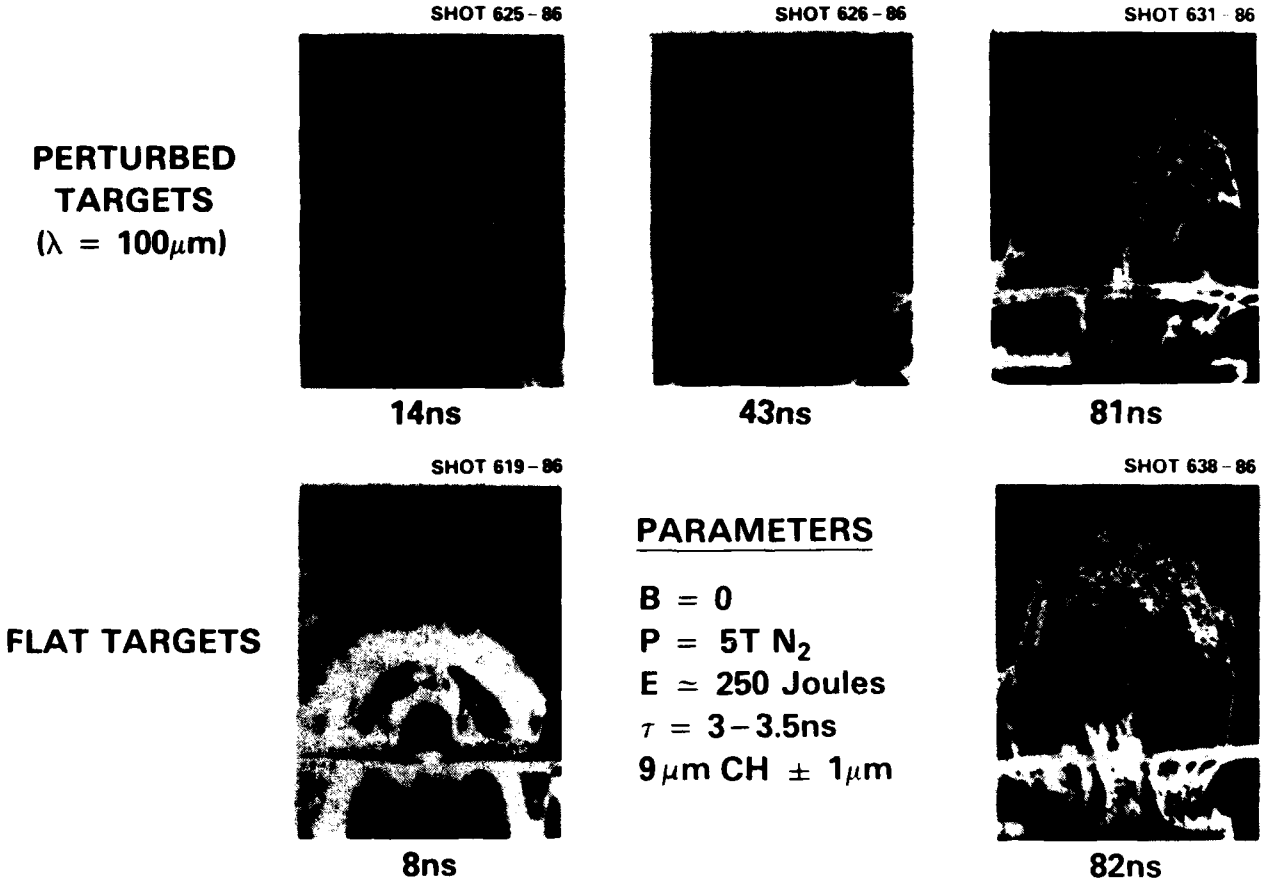

Figure 11. Sequences of turbulence formed as an accelerated perturbed target (top) and smooth target (bottom) expand behind the original target location.

CONCLUSIONS

It is clear that a wide variety of density structure is generated when a plasma expands into a magnetic field, another plasma, or both. The evolution of the structure, whether generated by instability, geometry, or by the laser beam itself impacts a wide variety of disciplines. The robust instability that occurs when a large ion Larmor radius plasma expands into a magnetic field has applicability to space physics situations, magnetic fusion confinement devices, as well as basic nonlinear plasma theory. We described a number of unusual phenomena that occur that should challenge the ingenuity of theorists. Aneurisms, which appear simple, are actually caused by several mechanisms. One mechanism studied in detail is laser-beam channel heating. This phenomena could be important in ICF reactors that use an ambient gas to reduce the first-wall impulse loading, as well as for laser beam guided particle beam schemes. The turbulence formed as dense highly-accelerated targets disassemble and expand is particularly striking. The dominant turbulent structure

appears to be independent of the Rayleigh-Taylor instability that has been observed during the laser-ablation acceleration process. Fourier analysis of the resulting turbulence, perhaps initiated by the Benard instability, shows a statistically well-developed large-amplitude turbulent plasma. This plasma may then become very useful as a test-bed to study fully developed turbulence theory.

This work was supported by the Defense Nuclear Agency.

REFERENCES

° Present address: Science Applications International Corporation, McLean, Virgina 22105.

1. B.H. Ripin, A.W. Ali, H.R. Griem, J. Grun, S.T. Kacenjar, C.K. Manka, E.A. McLean, A.N. Mostovych, S.P. Obenschain, and J.A. Stamper in: "Laser Plasma Interactions and Related Plasma Interactions, Vol 7" pgs 857-877, G. Miley and H. Hora, ed., Plenum Press, NY (1986).
2. A.B. Hassam and J.D. Huba, Geophys. Res. Letters 14, 60 (1987).
3. B.H. Ripin, E.A. McLean, C.K. Manka, C. Pawley, J.A.Stamper, T.A. Peyser, A.N. Mostovych, J. Grun, A.B. Hassam and J. Huba, Phys. Rev. Letters 59, 2299 (1987).
4. A.N. Mostovych, B.H. Ripin, and J.A. Stamper Bull. Am. Phys. Soc. 32, 1909 (1987); see also: Phys. Rev. Letters (1988).
5. G. Jellison and C. Parsons, Phys. Fluids 24, 1787 (1981).
6. J.A. Stamper, B.H. Ripin, R. Peterkin, Jr., R. F. Stellingwerf, (submitted to Phys. Fluids, 1987).
7. E.A. McLean, B.H. Ripin, and J.A. Stamper (to be published).
8. J. Grun, M.H. Emery, S.Kacenjar, C.B. Opal, E.A. McLean, S.P. Obenschian, B.H. Ripin, and A. Schmitt, Phys. Rev. Letters 53, 1352 (1984).
9. J. Grun, J.A. Stamper, and B.H. Ripin (to be published).
10. M. Kruskal and M. Schwarzchild, Proc. Roy. Soc. (London) A223, 348 (1954).
11. M.N. Rosenbluth and C.L. Longmire, Ann. Phys. (NY) 1 120 (1957).
12. H. Dickinson, W.H. Bostick, J.N. DiMarco, and S. Koslov, Phys. Fluids 5, 1048 (1962).
13. S. Okada, K. Sato, and T. Sekiguchi, Jap. J. App. Phys 20, 157 (1981).
14. Yu. P. Zakharov, A.M. Orishich, A.G. Ponomarenko, and V.G. Posukh, Sov. J. Plasma Phys. 12, 674 (1986).
15. M.N. Rosenbluth, N.A. Krall, and N. Rostoker, Nucl. Fusion Supplement Part 1, 143 (1967).
16. J.D. Huba, J.G. Lyon, and A.B. Hassam, Submitted to Phys. Rev. Letters (1987).
17. P.A. Bernhardt, R. Roussel-Dupre, M.B. Pongritz, G. Haerendel, A. Valenzuela, D.A. Gurnett, and R.R. Anderson, J. Geophys. Resh. 92, 5777 (1987).

18. B.H. Ripin, Bull. Am. Phys. Soc. 32, 1876 (1987).
19. B.H. Ripin, et al, (submitted to Phys. Fluids 1987).
20. C.K. Manka, C.J. Pawley, E.A. McLean, B.H. Ripin, T.A. Peyser, and J.A. Stamper, Bull. Am. Phys. Soc. 32 190 (1987).
21. N.A. Krall and P. C. Liewer, Phys. Rev. A 4, 2094 (1971)
22. D. Winske, (submitted to Phys. Fluids (1987).
23. J. Borovsky, Phys. Fluids 30, 2518 (1987).
24. C.K. Manka, T.A. Peyser, and B.H. Ripin (to be published).
25. M.C. Begelman, R.D. Blandford and M.J. Rees, Rev. Mod. Phys. 56, 255 (1984).
26. See for example: H. Azechi, Y. Sakagami, T. Yamanaka, C. Yamanaka, Appl. Phys. Letter 30 187 (1977); G.V. Sklizkov, in: "Laser Interaction and Related Plasma Phenomena, Vol 2" p 235-257, H.J. Schwarz and H. Hora, ed., Plenum Press, NY (1972).
27. J.G. Lyon, NRL Memo Report 5491 (1985).
28. C. Longmire, private communications.
29. J.L. Giuliani, NRL Memo Report 5420 (1985).
30. R.R. Peterson, and G. Moses, Nucl. Tech. and Fusion 4, 860 (1983).
31. R.H. Lehmberg, and S.P. Obenschain, Opt. Commun. 46, 27 (1983).
32. J.A. Stamper and B.H. Ripin, Phys. Rev. Letters 34, 138 (1975).
33. R.S. Bird, L.L. McKee, F. Schwirzke, and A.W. Cooper, Phys Rev A7, 1328 (1973); D.F. Edwards, V.V. Korobkin, S.L. Motilyov, and R.V. Serov, Phys Rev A16, 2437 (1977).
34. B.H. Ripin, R. DeCoste, S.P. Obenschain, S.E. Bodner, E.A. McLean, F.C. Young, R.R. Whitlock, C.M. Armstrong, J. Grun, J.A. Stamper, S.H. Gold, D.J. Nagel, R.H. Lehmberg, and J.M. McMahon, Phys Fluids 23 1012 (1979); 24 990 (E) (1981).
35. J. Grun, S.P. Obenschain, B.H. Ripin, R.R. Whitlock, E.A. McLean, J. Gardner, M.J. Herbst, and J.A. Stamper, Phys Fluids 26 588 (1983).
36. M. Rosen, R.H. Price, E.M. Campbell, D.W. Phillion, K.G. Esterbrook, B.F. Lasinski, J.M. Anerbach, S.P. Obenschain, E.A. McLean, R.R. Whitlock, and B.H. Ripin Phys Rev A 36, 347 (1987).
37. J. Grun, M.H. Emery, C.K. Manka, T.N. Lee, E.A. McLean, A. Mostovych, J. Stamper, S. Bodner, S.P. Obenschain, and B.H. Ripin Phys. Rev. Letters 58, 2672 (1987).

DISTRIBUTION LIST

AIR FORCE GEOPHYSICAL LAB.
Infrared Tech. Div. - LSI
Hanscom AFB, MA 01731
H. Gardiner

AUSTIN RESEARCH ASSOCIATES
1901 Rutland Avenue
Austin, TX 78758
R. Thompson

BERKELEY RESEARCH ASSOCIATES
P.O. Box 241
Berkeley, CA 94701
S. Brecht
C. Prettie
J. Workman
V. Thomas

CORNELL UNIVERSITY
Plasma Studies
309 Upson Hall
Cornell University
Ithaca, NY
D. Hammer

DEFENSE NUCLEAR AGENCY
Washington, D.C. 20305
Ms. J. Pierre
Dr. B. Prasad
Dr. K. Schwartz
Dr. G.W. Ullrick
Dr. T. Walsh
Dr. L.A. Wittwer
Dr. M. Owais

EOS TECHNOLOGIES INC.
606 Wilshire Blvd., Ste. 700
Santa Monica, CA 90407
B. Gabbard
R. LeLevier

FLUID SCIENCES
5871 Aylesboro Road
Pittsburg, PA 15217
N. Zabusky

JAYCOR
P.O. Box 85154
San Diego, CA 92138
J. Sperling
N. Krall

LOS ALAMOS NATIONAL LAB.
Los Alamos, NM 87545
J. Borovsky
S.P. Gary
P. Kadish
M. Pongratz
D. Sappenfield
G. Smith
D. Winske

MAXWELL - 8-Cubed Division
1800 Diagonal Road
Alexandria, VA 22314
K. Hain

MISSION RESEARCH CORPORATION
1720 Randolph Road, SE
Albuquerque, NM 87106
R. Peterkin
R. Stellingwerf
L. Sloan

MISSION RESEARCH CORPORATION
Drawer 719
Santa Barbara, CA 93102-0719
R. Bigoni
G. Bullock
F. Fajen
R. Goldflam
A. Gregersen
M. Hansman
R. Kilb
D. Landman
C. Longmire
D. Maloof
T. Mazurek
P. Ricchiazzi
D. Sowle
T. Old
W. White
E. Witt

MISSION RESEARCH CORPORATION
One Tara Blvd., Ste. 302
Nashua, NH 03062
R. Armstrong

NAVAL RESEARCH LABORATORY
Code
4700 W. Ali
4780 J. Fedder
4780 J. Giuliani
4732 H. Griem
4732 J. Grun
4780 J. Huba
4732 K. Kearney
4786 M. Keskinen
4732 T.N. Lee
4780 J. Lyon
4732 C. Manka
4732 E. McLean
4732 A. Mostovych
4780 M. Mulbrandon
4731 S. Obenschain
4700 S. Ossakow (26 cys.)
4732 C. Pawley
4732 T. Peyser
4732 B. Ripin (50 cys.)
4732 J. Stamper
4780 S. Zalesak

PLASMA RESEARCH CORPORATION
5850 Leesburg Pike #23
Falls Church, VA 22041
J. Guillory

2990 Main Street
Alameda, CA 94501
G. Dahlbacka

PHYSICAL RESEARCH, INC.
P.O. Box 30129
Santa Barbara, CA 93131
J.H. Thompson

PHYSICAL RESEARCH, INC.
134 Holiday Court, Ste. 309
Annapolis, MD 21401
H.C. Fitz

R&D ASSOCIATES
P.O. Box 9695
Marina Del Rey, CA 90295-2095
L. DeRaad
F. Gilmore

Director of Research
U.S. Naval Academy
Annopolis, MD 2 copy

SCIENCE APPLICATIONS INTERNAT. CORP.
1710 Goodridge Drive
McLean, VA 22101
E. Hyman
K. Papadopoulos

SCIENCE APPLICATIONS INTERNAT. CORP.
P.O. Box 2351
San Diego, CA 92038

SRI INTERNATIONAL
333 Ravenswood Ave.
Menlo Park, CA 94025
W. Chesnut

TOYON RESEARCH CORPROATION
P.O. Box 6890
Santa Barbara, CA 93111
J. Ise

UNIVERSITY OF CALIFORNIA AT LOS ANGELES
Department of Physics
Los Angeles, CA 90024
J.M. Cornwall
R. Stenzel
W. Gakelman
A.Y. Wong
J. Dawson

UNIVERSITY OF WISCONSIN
Fusion Technology Inst.
Madison, WS 53706
G. Moses
R. Peterson

VISIDYNE INC.
5 Corporate Place
South Bedford St.
Burlington, MA 01803
J. Carpenter

4730 - 25 copies
Please send remainder of copies to Code 4732.

Code 2628 22 copies

Records 1 copy

Code 1220 1 copy